



MIT Open Access Articles

Revisiting the HIP 41378 System with K 2 and Spitzer

The MIT Faculty has made this article openly available. ***Please share*** how this access benefits you. Your story matters.

As Published	10.3847/1538-3881/AB100C
Publisher	American Astronomical Society
Version	Final published version
Citable link	https://hdl.handle.net/1721.1/132402
Terms of Use	Article is made available in accordance with the publisher's policy and may be subject to US copyright law. Please refer to the publisher's site for terms of use.



Revisiting the HIP 41378 System with *K2* and *Spitzer*

David Berardo^{1,10}, Ian J. M. Crossfield¹, Michael Werner², Erik Petigura³, Jessie Christiansen⁴, David R. Ciardi⁴, Courtney Dressing⁵, Benjamin J. Fulton³, Varoujan Gorjian², Thomas P. Greene⁶, Kevin Hardegree-Ullman⁴, Stephen R. Kane⁷, John Livingston⁸, Farisa Morales², and Joshua E. Schlieder⁹

¹ Department of Physics, and Kavli Institute for Astrophysics and Space Research, Massachusetts Institute of Technology, Cambridge, MA 02139, USA
berardo@mit.edu

² Jet Propulsion Laboratory, California Institute of Technology, Pasadena, CA 91109, USA

³ Division of Geological and Planetary Sciences, California Institute of Technology, Pasadena, CA 91125, USA

⁴ NASA Exoplanet Science Institute, California Institute of Technology, M/S 100-22, 770 S. Wilson Avenue, Pasadena, CA, USA

⁵ Astronomy Department, University of California, Berkeley, CA 94720, USA

⁶ NASA Ames Research Center, Space Science and Astrobiology Division, MS 245-6, Moffett Field, CA 94035, USA

⁷ University of California Riverside, Department of Earth Sciences, Riverside, CA 92521, USA

⁸ Department of Astronomy, University of Tokyo, 7-3-1 Hongo, Bunkyo-ky, Tokyo 113-0033, Japan

⁹ Exoplanets and Stellar Astrophysics Laboratory, NASA Goddard Space Flight Center, Mail Code 667, 8800 Greenbelt Road, Greenbelt, MD 20771, USA

Received 2018 September 28; revised 2019 March 7; accepted 2019 March 12; published 2019 April 22

Abstract

We present new observations of the multiplanet system HIP 41378, a bright star ($V = 8.9$, $K_s = 7.7$) with five known transiting planets. Previous *K2* observations showed multiple transits of two Neptune-sized bodies and single transits of three larger planets ($R_p = 0.33R_J$, $0.47R_J$, $0.88R_J$). *K2* recently observed the system again in Campaign 18 (C18). We observe one new transit each of two of the larger planets d/f, giving maximal orbital periods of 1114/1084 days, as well as integer divisions of these values down to a lower limit of about 50 days. We use all available photometry to determine the eccentricity distributions of HIP 41378 d & f, finding that periods $\lesssim 300$ days require non-zero eccentricity. We check for overlapping orbits of planets d and f to constrain their mutual periods, finding that short periods ($P < 300$ days) for planet f are disfavored. We also observe transits of planets b and c with *Spitzer*/Infrared Array Camera (IRAC), which we combine with the *K2* observations to search for transit timing variations (TTVs). We find a linear ephemeris for planet b, but see a significant TTV signal for planet c. The ability to recover the two smaller planets with *Spitzer* shows that this fascinating system will continue to be detectable with *Spitzer*, *CHEOPS*, *TESS*, and other observatories, allowing us to precisely determine the periods of d and f, characterize the TTVs of planet c, recover the transits of planet e, and further enhance our view of this remarkable dynamical laboratory.

Key words: planetary systems – planets and satellites: detection – planets and satellites: gaseous planets

1. Introduction

Multiplanetary systems are just one of the many exciting discoveries that NASA's *Kepler* and *K2* missions have produced since the spacecraft's launch in 2009. These systems allow us to probe details regarding the formation, stability, and general structure of exoplanets, providing crucial data to motivate theories of exoplanet dynamics (e.g., Becker et al. 2015; Weiss et al. 2018). Although the *K2* mission is winding down, as we enter the next generation of exoplanet missions (*TESS*, *CHEOPS*, and eventually *JWST* and *ARIEL*), *K2* has proven its usefulness yet again with new observations of the multiplanet HIP 41378 system,¹¹ which it previously observed during Campaign 5 (C5; Vanderburg et al. 2016).

The initial observation revealed a rich system of two shorter period planets and three single-transit events, which were statistically significant as planets. As is often the case with such systems, additional data were needed to refine the orbital and physical properties of these outer planets and this was recently provided by *K2* during Campaign 18 (C18), which took both long- and short-cadence observations of HIP 41378. This system is not only one of a handful of known stars hosting five planets, but is also the second

brightest such system, with the host star having a *V*-band magnitude of 8.9 and *K* magnitude of 7.7—beaten only by the 55 Cancri system (Fischer et al. 2008)—making it a compelling target for future characterization if the periods of the larger planets can be precisely determined.

In Section 2 we discuss the various observations and analysis methods we use to further characterize the system. In Section 3 we provide updated stellar parameters for the host star based on *Gaia* data. Section 4 discusses the techniques and results of our dynamical study of the system, including eccentricity estimates. Finally in Section 5 we summarize our results and discuss the potential for future observations.

2. Photometric Observations and Analysis

Below we describe our time-series photometry analysis of HIP 41378, which includes photometry from *K2* (Section 2.1), *Spitzer* (Section 2.2), and a joint analysis of data sets from both telescopes (Section 2.3).

2.1. *K2*

HIP 41378 was originally observed by the *Kepler* space telescope during Campaign 5 of the *K2* mission for approximately 75 days. The system was then observed again during Campaign

¹⁰ NSERC Postgraduate Scholarship—Doctoral.

¹¹ R.A.: 08^h26^m27^s.85, decl.: +10^o04^m49^s.4.

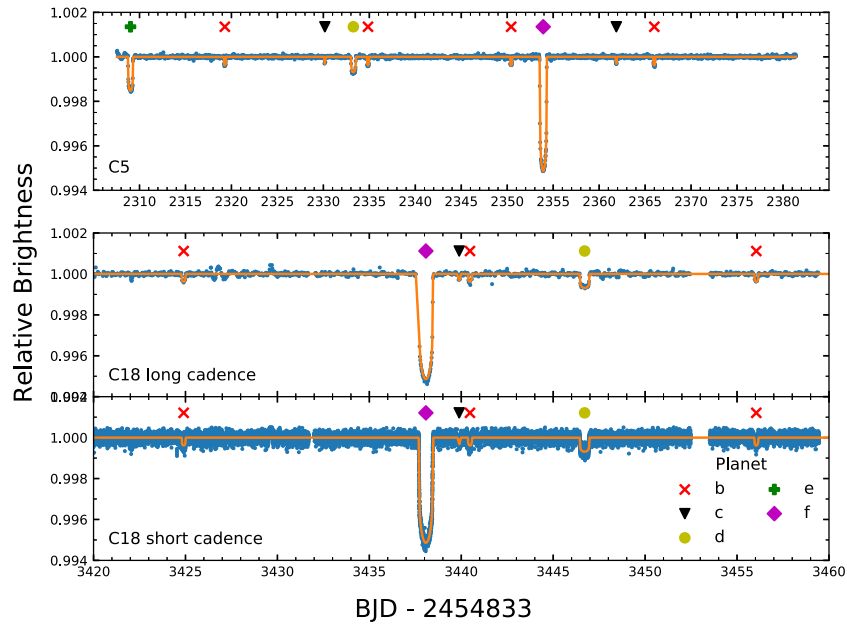


Figure 1. Light curves of HIP 41378 across all three observations (in blue) with transits of each planet highlighted. The orange line represents the best-fit model.

18 for approximately 50 days.^{12,13} Additionally, since the system was known to host planets, short-cadence (1 minute) photometry was collected during C18.¹⁴ The C5 data spans from $\text{BJD}_{\text{TDB}} = 2457140.5$ to 2457214.4 and is composed of 3378 frames, corresponding to observations every 30 minutes (with frames removed for thruster firing and other data quality flags). The C18 data spans $\text{BJD}_{\text{TDB}} = 2458251.5$ to 2458302.4 and consists of 2195 frames for the long-cadence data and 60,000 frames for the short-cadence data, again with frames removed due to quality issues. Thus there is a gap of approximately 1037 days between the end of C5 and the beginning of C18.

In the analysis that follows we use the fully detrended C5 light curve provided by Vanderburg et al. (2016). The calibrated C18 short- and long-cadence data are downloaded from MAST as target pixel files. These are then converted into light curves by performing simple aperture photometry, using a circular aperture centered on the center of light of each image to measure the stellar flux. The center of light is determined by taking the weighted mean of the flux of each pixel in the image. We then detrend both the long- and short-cadence light curves following the methods outlined in Vanderburg & Johnson (2014). Low frequency variations in each light curve are removed by first masking out points associated with transits, and then fitting a basis spline and dividing out the best fit to produce flattened light curves. Additionally, we trimmed the data to include only points within two transit durations from an expected transit center, to reduce analysis run times (Figure 1 shows the full short-cadence light curve). This is done in order to fit for individual planets without interference from the transit signals of the other planets in the system. This process produces 15 light curves, corresponding to three observations times of five planets. Before trimming, we also

check the light curves for signs of planet e, and while there additional transit-like signals in the light curve, none of them agree with the depth or duration of the known planets in the system and are likely due to detrending issues.

We derive a best-fit light curve model by fitting for each planet individually, using the *batman*¹⁵ (Kreidberg 2015) and *emcee*¹⁶ (Foreman-Mackey et al. 2013) Python packages to perform a Markov chain Monte Carlo (MCMC) analysis. When calculating light curves with *batman*, we divide the light curve into 30-minute intervals and then average over 10 points within each interval. This is done to simulate the 30-minute cadence of the *K2* data. For 1-minute cadence, it was found that averaging over 1-minute intervals changed the light curve at a level well below the scatter of the data, so averaging was not done. We evolve 150 walkers for 20,000 burn-in steps, followed by an additional 20,000 steps which are used to estimate the posterior values of the fitted parameters. These parameters are the center of transit t_0 , orbital period p , scaled planet radius r_p/r_s (where r_s is the radius of the host star), scaled semimajor axis a/r_s , orbital inclination i , and two limb-darkening parameters for a quadratic limb-darkening model, q_1 , q_2 (Kipping 2013). Additionally, the scatter σ of each light curve is left as a free parameter during the fit, producing three additional parameters (one for each observation). Thus the likelihood being maximized has the form

$$\text{Ln}\mathcal{L} = -\frac{1}{2} \sum_i \frac{(\text{flux}_i - \text{model}_i)^2}{\sigma_i^2} - 2\text{Ln}(\sigma_i), \quad (1)$$

where the index i runs over the three observations, the flux is the observed light curve, and the model is the calculated light curve given a set of orbital parameters. For all parameters except the limb-darkening coefficients, we use flat priors. We also use a flat prior for the limb-darkening coefficients when fitting for planet f. The high signal-to-noise of planet f produces

¹² While there was also partial overlap between the fields of Campaigns 5, 16, and 18, HIP 41378 was not observed in C16.

¹³ Long-cadence observations proposed for in C18 GO programs 3, 6, 27, 36, 47, 49, 65, 67, 901.

¹⁴ Short-cadence observations proposed for in C18 GO programs 6, 27, 36, 47.

¹⁵ <https://github.com/lkreidberg/batman>

¹⁶ <http://dfm.io/emcee/current/>

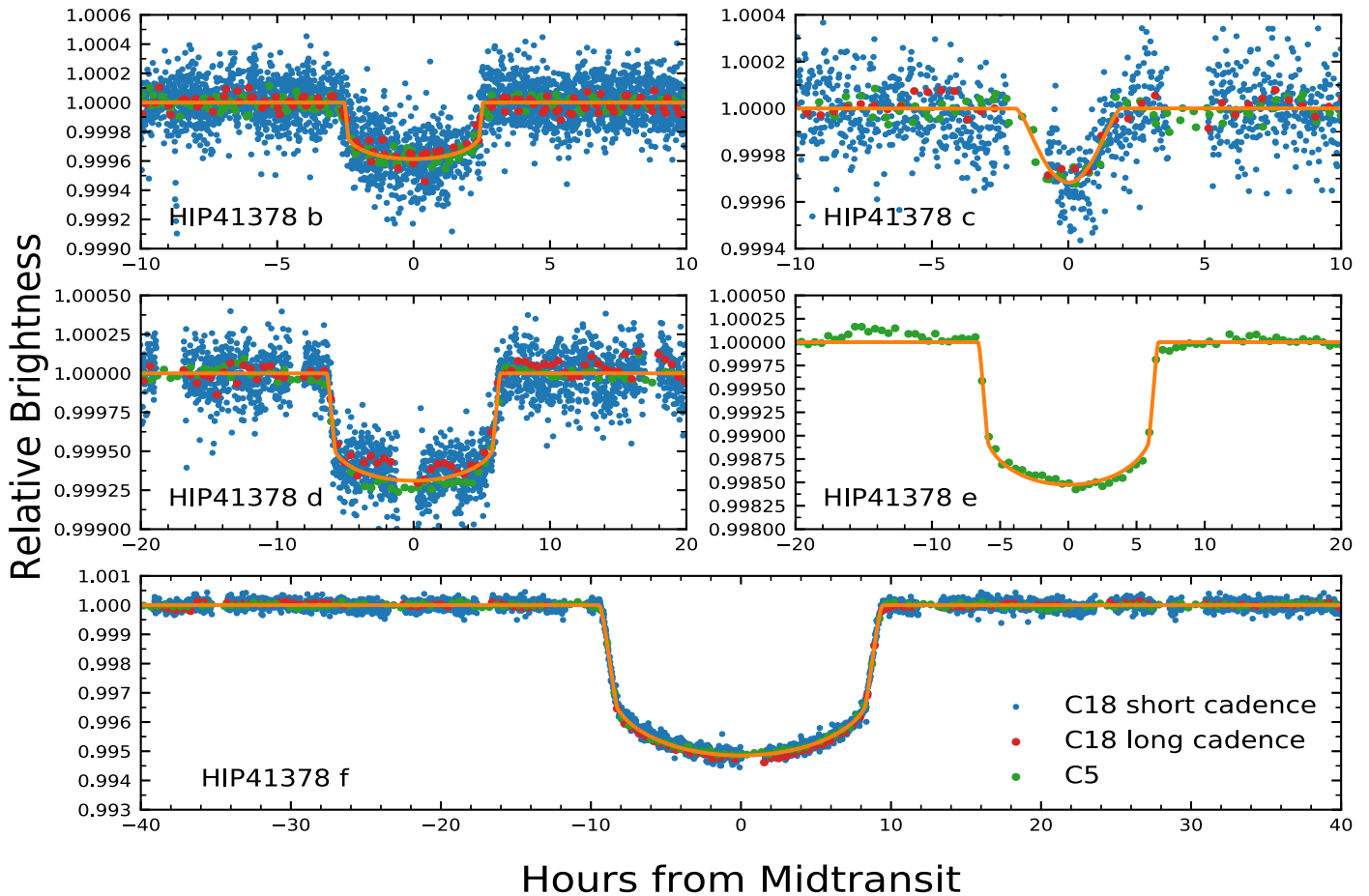


Figure 2. Transits of all five planets of HIP 41378, showing K2 data from C5 (green points) and C18 short- and long-cadence (blue and red points), along with our best-fit transit models (solid orange line). Planet e was not observed to transit during C18, and so we only show C5 data for it.

Table 1
K2 Fit Parameters

Planet Name	T_0 [BJD _{TDB} -2454833]	Period (days)	a/r_s	i degrees	r_p/r_s	q_1	q_2
HIP 41378 b	$2319.2818^{+0.0012}_{-0.0012}$	$15.572098^{+0.000018}_{-0.000019}$	21^{+2}_{-5}	$88.8^{+0.8}_{-1.4}$	$0.01843^{+0.0011}_{-0.00037}$	$0.463^{+0.015}_{-0.016}$	$0.064^{+0.028}_{-0.028}$
HIP 41378 c	$2330.1609^{+0.0023}_{-0.0027}$	$31.70648^{+0.00024}_{-0.00019}$	22^{+57}_{-7}	$87.5^{+2.2}_{-1.4}$	$0.0200^{+0.018}_{-0.0037}$	$0.456^{+0.017}_{-0.016}$	$0.050^{+0.030}_{-0.027}$
HIP 41378 d	$2333.2604^{+0.0017}_{-0.0017}$	$1113.4491^{+0.0018}_{-0.0018}$	533^{+81}_{-56}	$89.930^{+0.025}_{-0.018}$	$0.02560^{+0.0005}_{-0.0007}$	$0.444^{+0.015}_{-0.014}$	$0.028^{+0.022}_{-0.018}$
HIP 41378 e	$2309.0194^{+0.001}_{-0.001}$...	283^{+172}_{-177}	$89.910^{+0.22}_{-0.045}$	$0.03686^{+0.0011}_{-0.0008}$	$0.451^{+0.015}_{-0.015}$	$0.041^{+0.026}_{-0.024}$
HIP 41378 f	$2353.91423^{+0.00039}_{-0.00038}$	$1084.16156^{+0.00040}_{-0.00042}$	460^{+5}_{-4}	$89.98^{+0.009}_{-0.006}$	$0.06602^{+0.00017}_{-0.00016}$	$0.455^{+0.015}_{-0.014}$	$0.044^{+0.029}_{-0.026}$

Note. The limb-darkening parameters for planets b–e use the posterior values from the fit for planet f as Gaussian priors.

the tightest constraints on these parameters. For planets b through e, we then use the values of q_1 and q_2 found for planet f as Gaussian priors when running the MCMC. The resulting parameters are given in Table 1, where we quote the median value of the MCMC posterior distribution with 68% confidence intervals. The best-fit models are shown in Figure 1,¹⁷ and in Figure 2 we show the individual light curves for each planet, phase folded on their respective periods. In each case, the posterior value for the scatter is consistent with the out-of-transit standard deviation of the light curves.

¹⁷ For planets d and f we show the fit results assuming the maximal period, although other periods are possible as discussed in Section 4.

2.2. Spitzer

We also observed HIP 41378 using the 4.5 μm channel on *Spitzer*'s Infrared Array Camera (IRAC) as part of observing programs 11026 centered on BJD_{UTC} 2457606.932 and 13052 centered on BJD_{UTC} 2457790.680 (PI: Werner). The first observation coincides with an expected transit of HIP 41378 c while the second corresponds to an expected transit of HIP 41378 b.

We downloaded data from the *Spitzer* Heritage Archive¹⁸ and processed it into the light curves as follows. First, we used a median filter with a span of 10 frames to remove anomalous

¹⁸ <http://sha.ipac.caltech.edu/applications/Spitzer/SHA/>

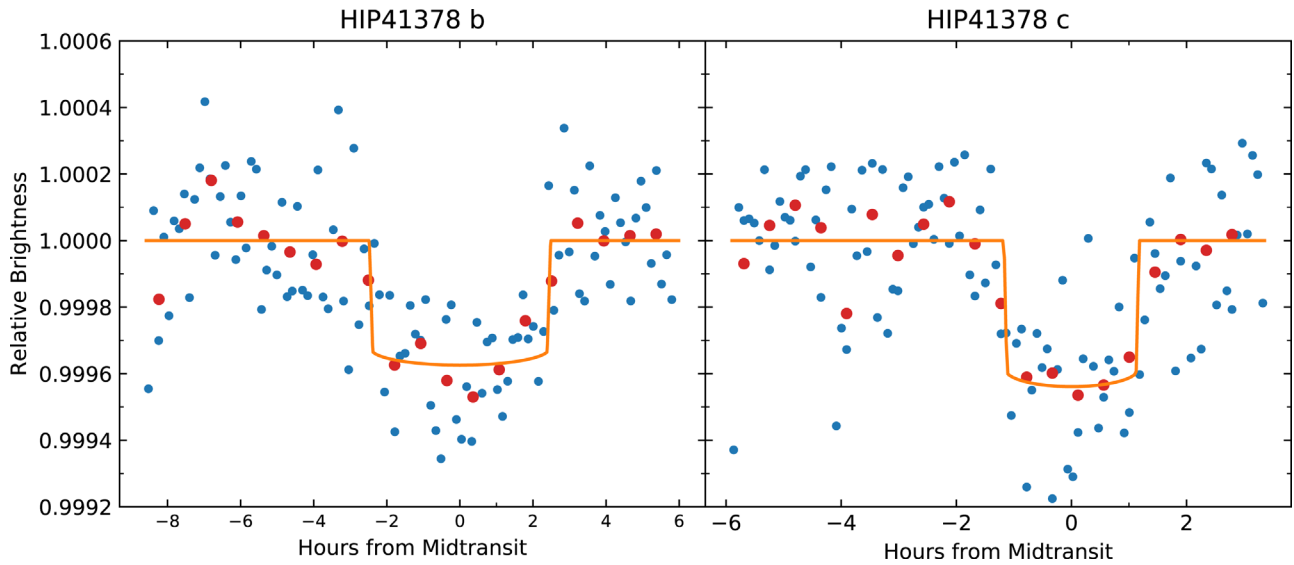


Figure 3. *Spitzer* photometry of HIP 41378b (left) and c (right). Blue dots show the (binned) photometry after removing systematic effects, red dots show the photometry binned by an additional factor of five, and the solid orange line shows the best-fit transit models.

Table 2
Spitzer Fit Parameters

Planet Name	T_0 [BJD _{TDB}]	Transit Depth (ppm)	r_p/r_s	a/r_s	i degrees
HIP 41378 b	$2457790.734^{+0.016}_{-0.0035}$	374^{+60}_{-65}	$0.0194^{+0.0015}_{-0.0016}$	22^{+3}_{-7}	$89.05^{+0.6}_{-1.3}$
HIP 41378 c	$2457606.985^{+0.0036}_{-0.0036}$	444^{+92}_{-95}	$0.0211^{+0.0022}_{-0.0022}$	85^{+14}_{-31}	$89.6^{+0.2}_{-0.6}$

pixels (flux values $>4\sigma$ from the median) due to cosmic rays and other effects. The centroid of each frame is then calculated in two ways, once by fitting a 2D Gaussian brightness profile, and again by calculating the center of light,

$$x_c = \frac{\sum_i f_i x_i}{\sum_i f_i}, y_c = \frac{\sum_i f_i y_i}{\sum_i f_i}, \quad (2)$$

where f_i is the flux of the i th column and x_i is the x-position for of the i th column (similarly for y and the rows). For each frame, we also calculated the background level by taking the flux in a 10×10 square in each corner of the image, fitting a Gaussian to the distribution of flux values, and taking the mean of the Gaussian to be the background level.

Light curves are then computed by summing up the flux in a circular aperture around the centroid and subtracting the appropriate amount of background flux, using the `photutils` (Bradley et al. 2018) Python package to account for partial pixels. We do this for apertures whose radii span from 1.8 to 3.4 pixels in 0.2 pixel increments, producing light curves for each combination of centroid method and aperture radius. For each of these, we determine a best-fit systematics model using the pixel-level decorrelation (PLD) technique (Deming et al. 2015). This method attempts to correct for the varying response of the pixels as the centroid moves around the CCD. Despite centroid motions of only about a tenth of a pixel, the magnitude of the intrapixel sensitivity, combined with the shallow depths of the transits (hundreds of parts per million) requires detrending of this effect in order to recover the transits.

We model the total flux as

$$S = \sum_i c_i f_i + DE(t) + ht + gt^2, \quad (3)$$

where D is the transit depth, $E(t)$ is the transit model, f_i is the flux of the i 'th pixel, c_i are coefficients correcting for the varying response of the pixels, and h and g are parameters used to model a quadratic time ramp. We perform a χ^2 minimization for each light curve to determine the best-fit parameters, and use the quality of the fits to determine which light curve to ultimately use. This is done by binning the residuals of the fit, plotting the standard deviation versus the bin factor, and choosing the one which has the closest slope to -0.5 (in log space), indicating the lowest amount of correlated noise. In addition to choosing the best light curve, we also bin down the data and see what effect this has on the results as well. This procedure ends up selecting a 2D Gaussian fit for centroiding, an aperture radius of 2.4 pixels, and a bin size of 200 points per bin.

Once we have chosen the best light curve for each observation, as for the *K2* data we run an MCMC chain in order to obtain posterior probability distributions and determine the errors for each parameter. The values being fit during the MCMC are the PLD pixel coefficients, the two time ramp parameters, the center of transit, the transit depth, as well as the orbital inclination and semimajor axis. The best-fit transit signals are shown in Figure 3 and the values are listed in Table 2.

Table 3
Individual Transit Centers for Planet b

Epoch	Observed [BJD _{TDB} -2454833]	Calculated [BJD _{TDB} -2454833]	$O - C$ (minutes)	Data Set
0	2319.2797 ^{+0.0008} _{-0.0006}	2319.2798	-0.1 ^{+1.2} _{0.9}	<i>K2</i> C5
1	2334.8499 ^{+0.0061} _{-0.001}	2334.8519	-2.9 ^{+8.7} _{1.5}	<i>K2</i> C5
2	2350.4187 ^{+0.0055} _{-0.0011}	2350.424	-7.7 ^{+8.0} _{1.6}	<i>K2</i> C5
3	2366.0033 ^{+0.001} _{-0.0039}	2365.9962	10.3 ^{+1.5} _{5.6}	<i>K2</i> C5
41	2957.734 ^{+0.016} _{-0.003}	2957.737	-4.0 ^{+23.2} _{4.3}	<i>Spitzer</i>
71	3424.90086 ^{+0.00021} _{-0.00021}	3424.9007	0.2 ^{+0.3} _{0.3}	<i>K2</i> C18
72	3440.47139 ^{+0.00021} _{-0.00021}	3440.47282	-2.1 ^{+0.3} _{0.3}	<i>K2</i> C18

Note. The calculated ephemeris is given by $t = 2319.27979 + (15.57213) \times E$, where E is the epoch of the transit. Errors on the calculated ephemeris are included in the errors of $O - C$ listed above.

Table 4
Individual Transit Centers for Planet c

Epoch	Observed [BJD _{TDB} -2454833]	Calculated [BJD _{TDB} -2454833]	$O - C$ (minutes)	Data Set
0	2330.16576 ^{+0.00245} _{-0.00272}	2330.15167	20.3 ^{+3.5} _{3.9}	<i>K2</i> C5
1	2361.86375 ^{+0.00297} _{-0.00284}	2361.85836	7.8 ^{+4.3} _{4.1}	<i>K2</i> C5
14	2773.986 ^{+0.0036} _{-0.0036}	2774.04529	-85.4 ^{+5.2} _{3.2}	<i>Spitzer</i>
35	3439.88676 ^{+0.0008} _{-0.00074}	3439.8857	1.5 ^{+1.2} _{1.1}	<i>K2</i> C18

Note. The calculated ephemeris is given by $t = 2330.15160 + (31.70669) \times E$, where E is the epoch of the transit. Errors on the calculated ephemeris are included in the errors of $O - C$ listed above.

We also performed analyses with two independent implementations of PLD, fitting the *Spitzer* data by itself (K. K. Hardegree-Ullman et al. 2019, in preparation) and also simultaneously with the *K2* data (Livingston et al. 2019), and the resulting parameter estimates were consistent. We find that for both planets, the values of semimajor axis and depth are consistent within the quoted errors between the *Spitzer* and *K2* values.

2.3. Joint *K2*+*Spitzer* Analysis

Combining the *K2* and *Spitzer* observations provides a total of eight transits of HIP 41378 b and four transit of HIP 41378 c, which allows us to check for transit timing variations (TTVs) that could indicate the presence of other non-transiting bodies and/or constrain the planets' masses. For both planets b and c, we keep fixed all of the best-fit parameters described in Section 2.1 and re-fit each transit individually across the C5, C18 short-cadence, and *Spitzer* data, allowing only the transit center to vary. For each planet we then fit a linear ephemeris to their epochs and observed transit times (taking into account their relative uncertainties), and plot the difference between the observed and calculated values in Figure 4 (these values are also listed in Tables 3 and 4). For planet b we discard the last observation, where we find a large offset in the transit center which we attribute to our detrending of the short-cadence C18 data. We feel comfortable discarding this point since we have two other transits of planet b during C18 to establish a long baseline with previous observations.

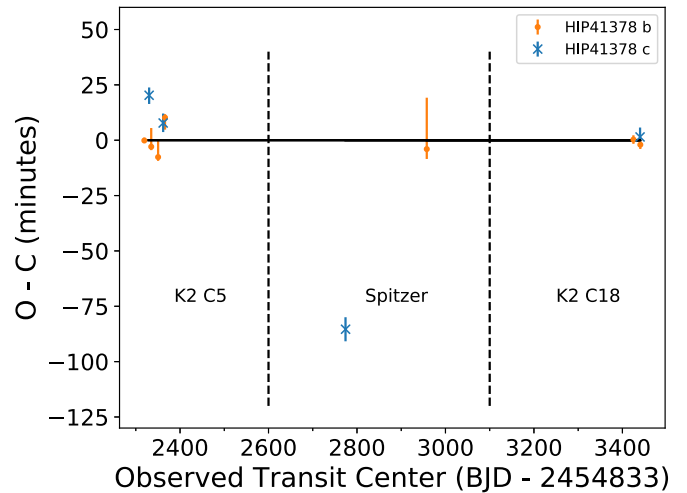


Figure 4. Transit timing variations plot for HIP 41378 b and c. Here we show the deviation from a linear ephemeris as a function of the measured transit center for the two inner short-period planets of the system. The dashed lines separate the three observations.

For HIP 41378 b we find results consistent with a linear ephemeris. For HIP 41378 c, we find that the the transit times are inconsistent with a linear ephemeris. While the systematic effects of the *Spitzer* observation make it difficult to obtain precise orbital parameters, as mentioned in Section 2.2 we have two external independent analyses of the observations which both produce similar TTV signals. We note while the C5 and

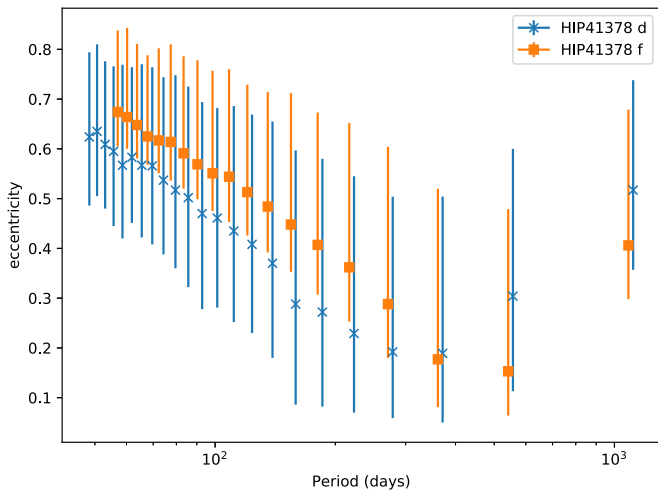


Figure 5. Possible eccentricities of HIP 41378 d (blue) and f (orange) from our photoeccentric analyses. We see a similar decreasing trend in eccentricity for both planets, indicating that lower eccentricities are consistent with longer periods.

Spitzer observations are broadly consistent with a linear ephemeris, although they predict that the transit of HIP 41378 c in C18 should be ~ 3 hr from where it is currently measured. Despite larger scatter in the C18 data than the C5 data, we do not believe that the transit center would shift by that amount. Additional transits are required to confirm the TTV signal seen here (see Figure 4 and Section 5.1).

3. Stellar Parameters

We derive an updated set of stellar parameters for HIP 41378 for use in our subsequent analysis. Vanderburg et al. (2016) report $T_{\text{eff}} = 6199 \pm 50$ K using spectroscopic techniques. We infer $T_{\text{eff}} = 6283 \pm 43$ by comparing the $B - V$, $V - K_s$, and $J - H$ colors to Table 5 of Pecaut & Mamajek (2013) and taking a weighted mean of the individual values from each color. We use the weighted mean of these two independent temperatures, along with the *Gaia* DR2 parallax (Gaia Collaboration et al. 2016, 2018) and the apparent stellar magnitudes in K_s and $W1$, as input parameters for the *isochrones* package (Morton 2015) with the MIST tracks (Choi et al. 2016). The computed parameters are $T_{\text{eff}} = 6226 \pm 43$ K, $R_* = 1.375 \pm 0.021 R_\odot$, $M_* = 1.168 \pm 0.072 M_\odot$, and $d = 106.58 \pm 0.65$ pc. None of these (except R_*) change by more than 1.5σ if we instead use the parallax with the magnitudes in V , B , J , H , K_s , $W1$, and $W2$. In this second analysis we find $R_* = 1.310 \pm 0.016 R_\odot$, so we take the mean and report an uncertainty that covers both values. Thus our final stellar radius is $1.343 \pm 0.032 R_\odot$. Our updated stellar parameters are listed in Table 5; all of the parameters are consistent with (but more precise than) those of Vanderburg et al. (2016).

We also derive stellar parameters using a high-resolution optical spectrum taken from Keck/HIRES, following the approach of Fulton & Petigura (2018). This spectrum implies $T_{\text{eff}} = 6266 \pm 100$, $R_* = 1.33 \pm 0.013 R_\odot$, $M_* = 1.17 \pm 0.030 M_\odot$, consistent with our analysis above.

Finally, we observe solar-like oscillations in the C18 short-cadence data. These could further refine the stellar parameters, but we defer that analysis for a subsequent paper.

Table 5
Updated HIP 41378 Parameters

Parameter	Units	Value	Comment
ϖ	mas	9.3799 ± 0.059	Gaia Collaboration et al.
R_*	R_\odot	1.343 ± 0.032	This work, Section 3
M_*	M_\odot	1.168 ± 0.072	This work, Section 3
ρ_*	g cm^{-3}	0.680 ± 0.064	This work, Section 3
T_{eff}	K	6226 ± 43	This work, Section 3

4. Dynamics

We used the transits of HIP 41378 f and HIP 41378 d to constrain each planet’s orbital eccentricity by applying the photoeccentric formalism of Dawson & Johnson (2012), using the same software and approach as described by Schlieder et al. (2016). This technique uses knowledge of the true stellar density ρ_* (calculated using our parameters in Section 3), combined with the derived stellar density from a fit assuming zero eccentricity $\rho_{*,\text{circ}}$,

$$\rho_{*,\text{circ}} = \frac{3\pi(a/r_s)^3}{GP^2} \quad (4)$$

in order to estimate the eccentricity of the orbit, where a/r_s is the scaled semimajor axis and P is the orbital period.

Since the two transits of HIP 41378 d/f have a gap of ~ 1000 days between them, there is a range of allowed periods that would produce the observed signals. The maximal possible period for the two planets, given by the delay between the observed transits, is 1114 days for planet d and 1084 days for planet f. The minimum possible periods are 48 days for planet d and 46 for planet f (shorter periods would have produced additional transits in either C5 or C18). Any fractional value of the longest period is also valid, and so this gives a range of 23 possible periods for both planets, for each of which we perform a photoeccentric analysis.¹⁹ We show the results of the five longest (and most plausible, as described below) periods for each planet in Tables 6 and 7, listing the maximum-likelihood values and 15.8% and 84.2% confidence intervals for all parameters. In addition to e and ω , we include the photoeccentric parameter g ,

$$g(e, \omega) = \frac{1 + e \sin \omega}{\sqrt{1 - e^2}} = \left(\frac{\rho_{*,\text{circ}}}{\rho_*} \right)^{1/3}. \quad (5)$$

See Figure 2 of Dawson et al. (2016) for the allowed relationships between e and ω for various values of g . For ρ_* , the stellar density, we use the value in Table 5. For $\rho_{*,\text{circ}}$, the density inferred solely from the transit light curve assuming a circular orbit (Seager & Mallén-Ornelas 2003), we take the posteriors computed directly from our MCMC analyses.

For both HIP 41378 f and HIP 41378 d, we find that g , e , and $e \sin \omega$ have fairly well-determined values. In contrast, the parameter ω and combination $e \cos \omega$ are only poorly constrained and so are not listed. Notable is that most possible periods are consistent with non-zero eccentricity at the $>2\sigma$, and even the lowest possible eccentricity is $1\sigma >$ than $e = 0$, indicating that both planets are most likely on eccentric orbits (see Figure 5).

¹⁹ None of the allowed periods predict transits of planet d or f during our *Spitzer* observations.

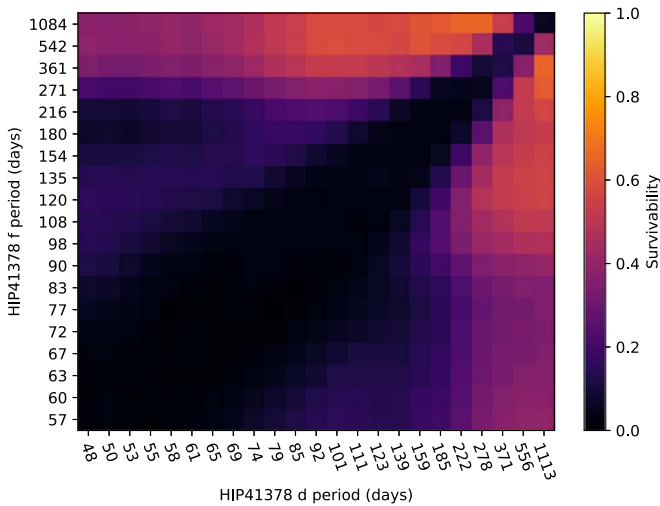


Figure 6. System stability of the HIP 41378 system for all possible periods of planets d and f (see Section 4.1). It is unlikely that both planets have short periods ($P \lesssim 300$ days), because then their orbits must be highly eccentric and they would interact with planet c. Similarly, these two outer planets will be unstable if they both have similar periods. We therefore find that one planet having a long period and the other having a shorter period is the most likely scenario.

Table 6
Photoeccentric Analysis for HIP 41378 D

Period	$g(e, \omega)$	e	$e \sin \omega$
1114	$1.47^{+0.229}_{-0.138}$	$0.517^{+0.221}_{-0.16}$	$0.262^{+0.136}_{-0.242}$
557	$1.154^{+0.171}_{-0.113}$	$0.304^{+0.296}_{-0.191}$	$0.07^{+0.135}_{-0.139}$
371	$1.022^{+0.135}_{-0.072}$	$0.189^{+0.315}_{-0.139}$	$-0.008^{+0.102}_{-0.128}$
278	$0.974^{+0.095}_{-0.096}$	$0.192^{+0.312}_{-0.133}$	$-0.066^{+0.099}_{-0.149}$
222	$0.936^{+0.106}_{-0.111}$	$0.229^{+0.316}_{-0.159}$	$-0.115^{+0.128}_{-0.171}$

Table 7
Photoeccentric Analysis for HIP 41378 F

Period	$g(e, \omega)$	e	$e \sin \omega$
1084	$1.337^{+0.031}_{-0.03}$	$0.406^{+0.273}_{-0.108}$	$0.217^{+0.061}_{-0.236}$
542	$1.059^{+0.026}_{-0.024}$	$0.153^{+0.326}_{-0.089}$	$0.035^{+0.031}_{-0.104}$
361	$0.931^{+0.023}_{-0.022}$	$0.177^{+0.343}_{-0.096}$	$-0.095^{+0.036}_{-0.11}$
271	$0.844^{+0.02}_{-0.019}$	$0.288^{+0.316}_{-0.108}$	$-0.2^{+0.039}_{-0.126}$
216	$0.784^{+0.019}_{-0.017}$	$0.362^{+0.29}_{-0.109}$	$-0.274^{+0.04}_{-0.13}$

4.1. Orbital Overlap

Using the results of the photoeccentric analysis, we perform a first-order stability analysis by calculating the possible orbits of planets d and f and excluding combinations of parameters where the planets' come within 3.5 mutual Hill radii of one another (Kane et al. 2016), with the mutual Hill radius of two objects given by

$$r_H = 0.5(a_1 + a_2)[(m_1 + m_2)/M]^{1/3}, \quad (6)$$

where we take M to be the mass of the host star (Table 5) and m_1/a_1 and m_2/a_2 are the masses/semimajor axes of planets d

and f. Since the masses of planets d and f are unknown, we conservatively choose the smallest reasonable masses. We use the publicly available `Forecaster` code (Chen & Kipping 2017) to estimate the probabilistic masses of the two planets given their radii ($r = 0.33R_J$, $0.88R_J$ for planets d and f, respectively). We then take the values 1σ below the median masses as our conservative mass estimate for the planets. We find masses of $0.02 M_J$ and $0.2 M_J$ for planets d and f, which results in a value of $r_H/(a_1 + a_2)$ of $\sim 3\%$.

Since the eccentricity and semimajor axis span a wide range of values, we draw samples from the posterior distributions obtained from the MCMC fits discussed in Section 2.1 and in our photoeccentric analysis. Since there are 20 possible periods for planet f and 23 for d, we run an MCMC analysis for each possible period, and perform a stability check for each pair of 20×23 periods. In this way, we calculate the likelihood for the two planets to have orbits with overlapping Hill spheres. In addition to checking for Hill sphere crossings, we also demand that any given orbit of HIP 41378 f and d does not overlap with the orbit of HIP 41378 c, which has a well-defined period and semimajor axis.

An important point is that in the analysis above we do not consider the effects of the fifth planet HIP 41378 e. Due to only observing a single transit, we are not able to constrain its period or semimajor axis and so elect to disregard any effects it may have on the system.

We show the results of this analysis in Figure 6, with darker colors indicating a higher probability of overlap. At low periods ($p \lesssim 300$ days) there is a higher chance of overlap than long periods. This is likely due to the fact that at low periods, the photoeccentric analysis predicts increasing eccentricities, shown in Figure 5, making it much more likely that the orbits will overlap with either each other or with planet c. Additionally, the dark diagonal indicates that similar periods for f and d are highly disfavored.

In the most favored scenario (i.e., the one with the highest relative survivability), HIP 41378 d has $p = 1114$ days and HIP 41378 f has $p = 361$ or 542 days; Figure 5 shows that this scenario also corresponds to the lowest eccentricities for these two planets.

5. Discussion

We analyze new transits of four out of the five planets in the HIP 41378 system using *K2* data, two of which previously only had a single observed transit. We study the possible periods of the two planets, and also employ a photoeccentric analysis to study their eccentricity distributions. We find that the eccentricity of the planets increases with decreasing period, however this implies that their orbits will overlap and so disfavors short periods.

We also observe one additional transit each of planets b and c using *Spitzer* IRAC, providing a sufficient baseline to check for TTVs. For HIP 41378 b we find all observations consistent with a linear ephemeris ($t_0 = 2457152.281 \pm 0.015$ BJD & $p = 15.572119 \pm 0.000022$ days). For HIP 41378 c the *Spitzer* photometry, which occurs roughly at the midpoint between the *K2* campaigns, implies a transit deviation on the order of

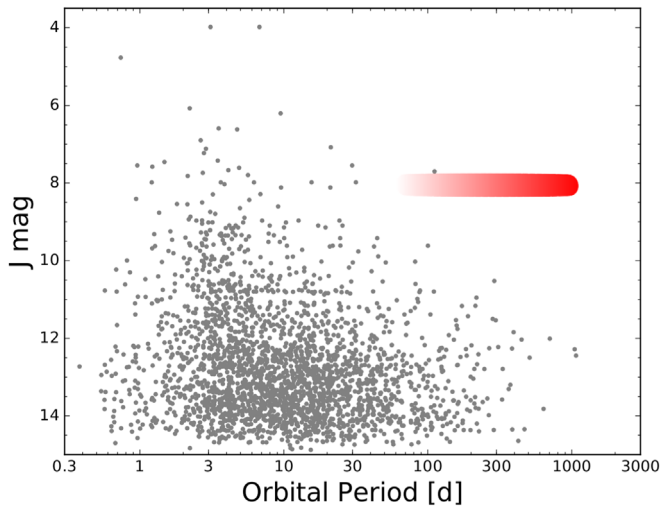


Figure 7. HIP 41378 d and f in context: orbital period vs. J mag for all known transiting planets. The shaded red lozenge approximately indicates HIP 41378 d and f—whatever the orbital periods of these planets, this system is several magnitudes brighter than any comparable system.

50–100 minutes. Our *Spitzer* analysis is consistent with two independent, external analyses performed on the same data set.

5.1. Follow-up Opportunities

For HIP 41378 f, it might seem that such a long-period planet around such a bright star would be an attractive target for high-contrast characterization. Unfortunately, the system lies 106 pc away and so even a 1084-day (2.2 au) orbit places HIP 41378 f just 20 mas from its host star. Assuming a Jupiter-like geometric albedo of 0.35 and a Lambertian phase function, the most favorable planet/star contrasts define a locus from 6×10^{-8} at 6 mas (for a 217-day period), to 7×10^{-9} at 18 mas (for $P = 1084$ days). These values appear to lie just beyond the regime accessible to proposed high-contrast instruments on the next generation of ground-based telescopes (Beuzit et al. 2006; Macintosh et al. 2006; Crossfield 2016). Nonetheless, that the planets could come so close to detection bodes well for high-contrast characterization of long-period planets around nearby stars discovered via single transits in *TESS* photometry (Villanueva et al. 2018). Additionally, we find that the *James Webb Space Telescope* (*JWST*) transmission spectroscopy of the planets is possible at a signal-to-noise ratio of 8–10 for a cloud-free H₂-dominated atmosphere if the systematic noise can be kept extremely low (~ 5 ppm). While this seems like a strict requirement, it is nonetheless interesting

to note that such measurements may be feasible for any or all of the larger planets in the system, if their periods can be properly constrained.

The two outer planets d and f also fall into a less-widely appreciated class of planets, transiting giants on ultra-long periods (T-GULPs). T-GULPs are those planets with the longest orbital periods, orbiting at the widest separations, and consequently having the lowest known equilibrium temperatures of any known transiting planet. Figure 7 lists the known T-GULPs (see also Table 7 of Beichman et al. 2018 for a list of their properties). Interestingly, few other T-GULPs are known to be in multiplanet systems, and no others orbit stars as bright as HIP 41378 ($V = 9$ mag). Whatever their true periods, HIP 41378 d and f (together with their sibling planets) form an exceptional system that will be studied for many years to come.

The sample of T-GULPs will likely grow only slowly in the years to come, since *TESS* and other future transit missions will not observe any single field of view nearly as long as *Kepler*. Only through the extraordinary endurance of *K2* was this observatory able to redetect the transits of HIP 41378 d and f. *TESS* will find a few longer-period planets in its continuous viewing zones (e.g., Sullivan et al. 2015), but only through an extended mission can the population of truly long-period T-GULPs be substantially expanded.

Because the typical T-GULP has only a few transits observed, the effects of additional perturbing bodies or simple ephemeris drift could eventually result in many of these rare specimens being lost. The situation is even more complicated for HIP 41378 d and f, since only a finite range of possible periods are known. Such long-duration transits (13 hr for planet d and 19 hr for planet f) are challenging to observe from the ground (though it can be done; e.g., Shporer et al. 2010). In contrast, space-based transit photometry is a proven technique for producing high-quality system parameters. We have shown here that *Spitzer* is capable of retrieving transits of the two smaller planets in the system, measuring their transit times to within a few minutes. This implies that it will be easy to observe planets d and f, larger planets with longer transit durations.

By employing a strategic observing strategy (i.e., observing during the fourth longest period to simultaneously check for the eighth and sixteenth longest periods), and using the mutual-likelihood plot of the planet periods (Figure 6), it may be possible to pin down the periods of both HIP 41378 d and f with only a few additional measurements. We list the future expected transits for the longest periods of each planet in Tables and 8 and 9.

Table 8
Future Transit Windows for HIP 41378 d

Period (days)	T_0 [BJD _{TDB} -2454833]	Start (UT)	Midpoint (UT)	End (UT)
1113.45	4560.1586 $^{+0.0022}_{-0.0022}$	2021 Jun 27 09:28:32	2021 Jun 27 15:48:21	2021 Jun 27 22:07:47
556.72	4003.434 $^{+0.0014}_{-0.0014}$	2019 Dec 18 16:05:13	2019 Dec 18 22:24:53	2019 Dec 19 04:44:23
371.15	3817.8591 $^{+0.0011}_{-0.0011}$	2019 Jun 16 02:17:27	2019 Jun 16 08:37:09	2019 Jun 16 14:56:33
278.36	3725.0717 $^{+0.001}_{-0.001}$	2019 Mar 15 07:23:12	2019 Mar 15 13:43:11	2019 Mar 15 20:02:55
222.69	3669.3992 $^{+0.0009}_{-0.0009}$	2019 Jan 18 15:15:19	2019 Jan 18 21:34:53	2019 Jan 19 03:54:17
185.57	3632.2843 $^{+0.0009}_{-0.0009}$	2018 Dec 12 12:29:47	2018 Dec 12 18:49:21	2018 Dec 13 01:08:38
159.06	3605.7736 $^{+0.0008}_{-0.0009}$	2018 Nov 16 00:14:43	2018 Nov 16 06:34:01	2018 Nov 16 12:53:01
159.06	3764.8378 $^{+0.001}_{-0.001}$	2019 Apr 24 01:47:08	2019 Apr 24 08:06:26	2019 Apr 24 14:25:25
139.18	3585.8906 $^{+0.0009}_{-0.0009}$	2018 Oct 27 03:02:44	2018 Oct 27 09:22:24	2018 Oct 27 15:41:57
139.18	3725.0717 $^{+0.001}_{-0.001}$	2019 Mar 15 07:23:35	2019 Mar 15 13:43:14	2019 Mar 15 20:02:47
123.72	3570.426 $^{+0.0009}_{-0.0008}$	2018 Oct 11 15:53:31	2018 Oct 11 22:13:24	2018 Oct 12 04:33:04
123.72	3694.1425 $^{+0.001}_{-0.001}$	2019 Feb 12 09:05:23	2019 Feb 12 15:25:15	2019 Feb 12 21:44:56
111.34	3558.0544 $^{+0.0009}_{-0.0008}$	2018 Sep 29 06:58:25	2018 Sep 29 13:18:16	2018 Sep 29 19:37:49
111.34	3669.3993 $^{+0.001}_{-0.0009}$	2019 Jan 18 15:15:06	2019 Jan 18 21:34:56	2019 Jan 19 03:54:29
111.34	3780.7442 $^{+0.0011}_{-0.0011}$	2019 May 09 23:31:46	2019 May 10 05:51:37	2019 May 10 12:11:09
101.22	3649.1547 $^{+0.0009}_{-0.0009}$	2018 Dec 29 09:23:17	2018 Dec 29 15:42:46	2018 Dec 29 22:02:04
101.22	3750.3774 $^{+0.001}_{-0.001}$	2019 Apr 9 14:43:54	2019 Apr 9 21:03:23	2019 Apr 10 03:22:40
92.79	3632.2843 $^{+0.0009}_{-0.0009}$	2018 Dec 12 12:30:11	2018 Dec 12 18:49:22	2018 Dec 13 01:08:15
92.79	3725.0717 $^{+0.001}_{-0.001}$	2019 Mar 15 07:24:05	2019 Mar 15 13:43:15	2019 Mar 15 20:02:07
85.65	3618.0093 $^{+0.0009}_{-0.0009}$	2018 Nov 28 05:53:57	2018 Nov 28 12:13:25	2018 Nov 28 18:32:42
85.65	3703.6593 $^{+0.001}_{-0.001}$	2019 Feb 21 21:29:52	2019 Feb 22 03:49:19	2019 Feb 22 10:08:36
85.65	3789.3092 $^{+0.0011}_{-0.0011}$	2019 May 18 13:05:47	2019 May 18 19:25:13	2019 May 19 01:44:29
79.53	3605.7736 $^{+0.0009}_{-0.0009}$	2018 Nov 16 00:14:24	2018 Nov 16 06:33:59	2018 Nov 16 12:53:22
79.53	3685.3057 $^{+0.0009}_{-0.001}$	2019 Feb 3 13:00:36	2019 Feb 3 19:20:11	2019 Feb 04 01:39:34
79.53	3764.8378 $^{+0.001}_{-0.0011}$	2019 Apr 24 01:46:49	2019 Apr 24 08:06:23	2019 Apr 24 14:25:45
74.23	3595.1693 $^{+0.0008}_{-0.0008}$	2018 Nov 5 09:44:06	2018 Nov 5 16:03:47	2018 Nov 05 22:23:16
74.23	3669.3992 $^{+0.0009}_{-0.0009}$	2019 Jan 18 15:15:13	2019 Jan 18 21:34:53	2019 Jan 19 03:54:23
74.23	3743.6292 $^{+0.001}_{-0.001}$	2019 Apr 2 20:46:20	2019 Apr 3 03:06:00	2019 Apr 03 09:25:30
69.59	3585.8906 $^{+0.0009}_{-0.0009}$	2018 Oct 27 03:02:47	2018 Oct 27 09:22:25	2018 Oct 27 15:41:48
69.59	3655.4811 $^{+0.0009}_{-0.0009}$	2019 Jan 4 17:13:13	2019 Jan 4 23:32:50	2019 Jan 05 05:52:14
69.59	3725.0717 $^{+0.001}_{-0.001}$	2019 Mar 15 07:23:39	2019 Mar 15 13:43:15	2019 Mar 15 20:02:39
69.59	3794.6623 $^{+0.0011}_{-0.0011}$	2019 May 23 21:34:04	2019 May 24 03:53:40	2019 May 24 10:13:04
65.5	3577.7034 $^{+0.0008}_{-0.0008}$	2018 Oct 18 22:33:18	2018 Oct 19 04:52:57	2018 Oct 19 11:12:24
65.5	3643.2005 $^{+0.0009}_{-0.0009}$	2018 Dec 23 10:29:00	2018 Dec 23 16:48:39	2018 Dec 23 23:08:05
65.5	3708.6975 $^{+0.001}_{-0.001}$	2019 Feb 26 22:24:42	2019 Feb 27 04:44:20	2019 Feb 27 11:03:46
65.5	3774.1945 $^{+0.001}_{-0.0011}$	2019 May 3 10:20:23	2019 May 3 16:40:01	2019 May 03 22:59:27
61.86	3570.426 $^{+0.0008}_{-0.0008}$	2018 Oct 11 15:53:42	2018 Oct 11 22:13:23	2018 Oct 12 04:32:53
61.86	3632.2843 $^{+0.0009}_{-0.0009}$	2018 Dec 12 12:29:38	2018 Dec 12 18:49:19	2018 Dec 13 01:08:49
61.86	3694.1425 $^{+0.001}_{-0.001}$	2019 Feb 12 09:05:34	2019 Feb 12 15:25:14	2019 Feb 12 21:44:45
61.86	3756.0008 $^{+0.001}_{-0.001}$	2019 Apr 15 05:41:31	2019 Apr 15 12:01:10	2019 Apr 15 18:20:40
58.6	3563.9146 $^{+0.001}_{-0.0009}$	2018 Oct 5 03:37:27	2018 Oct 5 09:56:58	2018 Oct 05 16:16:26
58.6	3622.5171 $^{+0.001}_{-0.001}$	2018 Dec 2 18:05:11	2018 Dec 3 00:24:41	2018 Dec 03 06:44:10
58.6	3681.1197 $^{+0.0011}_{-0.001}$	2019 Jan 30 08:32:54	2019 Jan 30 14:52:24	2019 Jan 30 21:11:53
58.6	3739.7223 $^{+0.0012}_{-0.0011}$	2019 Mar 29 23:00:38	2019 Mar 30 05:20:07	2019 Mar 30 11:39:37
55.67	3558.0544 $^{+0.0008}_{-0.0008}$	2018 Sep 29 06:58:51	2018 Sep 29 13:18:16	2018 Sep 29 19:37:25
55.67	3613.7268 $^{+0.0009}_{-0.0009}$	2018 Nov 23 23:07:11	2018 Nov 24 05:26:37	2018 Nov 24 11:45:45

Table 8
(Continued)

Period (days)	T_0 [BJD _{TDB} -2454833]	Start (UT)	Midpoint (UT)	End (UT)
55.67	3669.3993 ^{+0.0009} _{-0.0009}	2019 Jan 18 15:15:32	2019 Jan 18 21:34:57	2019 Jan 19 03:54:05
55.67	3725.0717 ^{+0.001} _{-0.001}	2019 Mar 15 07:23:52	2019 Mar 15 13:43:17	2019 Mar 15 20:02:25
53.02	3605.7736 ^{+0.0009} _{-0.0009}	2018 Nov 16 00:14:13	2018 Nov 16 06:33:56	2018 Nov 16 12:53:25
53.02	3658.795 ^{+0.0009} _{-0.0009}	2019 Jan 8 00:45:00	2019 Jan 8 07:04:43	2019 Jan 08 13:24:12
53.02	3711.8163 ^{+0.001} _{-0.001}	2019 Mar 2 01:15:48	2019 Mar 2 07:35:31	2019 Mar 02 13:55:00
53.02	3764.8377 ^{+0.001} _{-0.0011}	2019 Apr 24 01:46:36	2019 Apr 24 08:06:19	2019 Apr 24 14:25:48
50.61	3598.5433 ^{+0.0009} _{-0.0011}	2018 Nov 8 18:42:30	2018 Nov 9 01:02:20	2018 Nov 09 07:21:29
50.61	3649.1546 ^{+0.001} _{-0.0011}	2018 Dec 29 09:22:48	2018 Dec 29 15:42:38	2018 Dec 29 22:01:47
50.61	3699.7659 ^{+0.001} _{-0.0012}	2019 Feb 18 00:03:07	2019 Feb 18 06:22:56	2019 Feb 18 12:42:05
50.61	3750.3773 ^{+0.0011} _{-0.0013}	2019 Apr 9 14:43:25	2019 Apr 9 21:03:14	2019 Apr 10 03:22:23
48.41	3591.9419 ^{+0.0009} _{-0.0009}	2018 Nov 2 04:16:48	2018 Nov 2 10:36:22	2018 Nov 02 16:55:41
48.41	3640.3528 ^{+0.0009} _{-0.0009}	2018 Dec 20 14:08:25	2018 Dec 20 20:27:58	2018 Dec 21 02:47:17
48.41	3688.7636 ^{+0.001} _{-0.001}	2019 Feb 7 00:00:01	2019 Feb 7 06:19:34	2019 Feb 07 12:38:53
48.41	3737.1744 ^{+0.001} _{-0.001}	2019 Mar 27 09:51:37	2019 Mar 27 16:11:10	2019 Mar 27 22:30:29

Table 9
Future Transit Windows of HIP 41378 f

Period (days)	T_0 [BJD _{TDB} -2454833]	Start (UT)	Midpoint (UT)	End (UT)
1084.16	4522.23776 ^{+0.00048} _{-0.00047}	2021 May 20 08:16:43	2021 May 20 17:42:22	2021 May 21 03:08:00
542.08	3980.15685 ^{+0.00029} _{-0.0003}	2019 Nov 25 06:20:14	2019 Nov 25 15:45:52	2019 Nov 26 01:11:29
361.39	3799.46322 ^{+0.00024} _{-0.00024}	2019 May 28 13:41:25	2019 May 28 23:07:02	2019 May 29 08:32:38
271.04	3709.1164 ^{+0.00022} _{-0.00022}	2019 Feb 27 05:21:59	2019 Feb 27 14:47:36	2019 Feb 28 00:13:14
216.83	3654.90831 ^{+0.0002} _{-0.0002}	2019 Jan 4 00:22:21	2019 Jan 4 09:47:58	2019 Jan 04 19:13:34
180.69	3618.76958 ^{+0.00019} _{-0.00019}	2018 Nov 28 21:02:35	2018 Nov 29 06:28:11	2018 Nov 29 15:53:48
180.69	3799.46321 ^{+0.00024} _{-0.00024}	2019 May 28 13:41:24	2019 May 28 23:07:01	2019 May 29 08:32:38
154.88	3592.9562 ^{+0.00019} _{-0.00018}	2018 Nov 3 01:31:21	2018 Nov 3 10:56:55	2018 Nov 03 20:22:30
154.88	3747.83646 ^{+0.00023} _{-0.00022}	2019 Apr 6 22:38:54	2019 Apr 7 08:04:29	2019 Apr 07 17:30:04
135.52	3573.59617 ^{+0.00019} _{-0.00018}	2018 Oct 14 16:52:51	2018 Oct 15 02:18:29	2018 Oct 15 11:44:07
135.52	3709.1164 ^{+0.00022} _{-0.00021}	2019 Feb 27 05:21:59	2019 Feb 27 14:47:36	2019 Feb 28 00:13:14
120.46	3558.53838 ^{+0.00018} _{-0.00017}	2018 Sep 29 15:29:40	2018 Sep 30 00:55:15	2018 Sep 30 10:20:52
120.46	3679.0008 ^{+0.00021} _{-0.0002}	2019 Jan 28 02:35:33	2019 Jan 28 12:01:09	2019 Jan 28 21:26:46
120.46	3799.46323 ^{+0.00024} _{-0.00023}	2019 May 28 13:41:27	2019 May 28 23:07:02	2019 May 29 08:32:39
108.42	3654.90831 ^{+0.0002} _{-0.0002}	2019 Jan 4 00:22:20	2019 Jan 4 09:47:57	2019 Jan 04 19:13:35
108.42	3763.32449 ^{+0.00023} _{-0.00023}	2019 Apr 22 10:21:38	2019 Apr 22 19:47:15	2019 Apr 23 05:12:52
98.56	3635.19628 ^{+0.0002} _{-0.00019}	2018 Dec 15 07:17:01	2018 Dec 15 16:42:38	2018 Dec 16 02:08:15
98.56	3733.75644 ^{+0.00022} _{-0.00022}	2019 Mar 23 20:43:39	2019 Mar 24 06:09:16	2019 Mar 24 15:34:53
90.35	3618.76958 ^{+0.00019} _{-0.00019}	2018 Nov 28 21:02:37	2018 Nov 29 06:28:11	2018 Nov 29 15:53:46
90.35	3709.1164 ^{+0.00022} _{-0.00021}	2019 Feb 27 05:22:02	2019 Feb 27 14:47:37	2019 Feb 28 00:13:11
90.35	3799.46322 ^{+0.00024} _{-0.00024}	2019 May 28 13:41:27	2019 May 28 23:07:02	2019 May 29 08:32:36
83.4	3604.87008 ^{+0.00019} _{-0.00019}	2018 Nov 14 23:27:17	2018 Nov 15 08:52:54	2018 Nov 15 18:18:31
83.4	3688.26714 ^{+0.00021} _{-0.00021}	2019 Feb 06 08:59:03	2019 Feb 06 18:24:40	2019 Feb 07 03:50:17
83.4	3771.6642 ^{+0.00023} _{-0.00023}	2019 Apr 30 18:30:49	2019 May 1 03:56:26	2019 May 01 13:22:04
77.44	3592.95633 ^{+95.31082} _{-0.00026}	2018 Nov 3 01:31:41	2018 Nov 3 10:57:07	2018 Nov 03 20:22:55
77.44	3670.39648 ^{+101.26775} _{-0.00029}	2019 Jan 19 12:05:28	2019 Jan 19 21:30:55	2019 Jan 20 06:56:42

Table 9
(Continued)

Period (days)	T_0 [BJD _{TDB} -2454833]	Start (UT)	Midpoint (UT)	End (UT)
77.44	3747.83662 $^{+107.22467}_{-0.00031}$	2019 Apr 6 22:39:16	2019 Apr 7 08:04:43	2019 Apr 07 17:30:30
72.28	3582.63095 $^{+87.76528}_{-0.00023}$	2018 Oct 23 17:43:07	2018 Oct 24 03:08:34	2018 Oct 24 12:34:21
72.28	3654.90842 $^{+92.92794}_{-0.00026}$	2019 Jan 4 00:22:39	2019 Jan 4 09:48:07	2019 Jan 04 19:13:54
72.28	3727.18588 $^{+98.09059}_{-0.00028}$	2019 Mar 17 07:02:12	2019 Mar 17 16:27:40	2019 Mar 18 01:53:26
72.28	3799.46335 $^{+103.25324}_{-0.00031}$	2019 May 28 13:41:44	2019 May 28 23:07:13	2019 May 29 08:32:59
67.76	3573.59617 $^{+0.00019}_{-0.0002}$	2018 Oct 14 16:52:51	2018 Oct 15 02:18:29	2018 Oct 15 11:44:05
67.76	3641.35628 $^{+0.0002}_{-0.00021}$	2018 Dec 21 11:07:24	2018 Dec 21 20:33:02	2018 Dec 22 05:58:39
67.76	3709.11639 $^{+0.00022}_{-0.00023}$	2019 Feb 27 05:21:58	2019 Feb 27 14:47:36	2019 Feb 28 00:13:12
67.76	3776.87651 $^{+0.00024}_{-0.00025}$	2019 May 5 23:36:32	2019 May 6 09:02:10	2019 May 06 18:27:46
63.77	3565.6244 $^{+0.00018}_{-0.00018}$	2018 Oct 6 17:33:30	2018 Oct 7 02:59:08	2018 Oct 07 12:24:45
63.77	3629.39862 $^{+0.00019}_{-0.00019}$	2018 Dec 9 12:08:23	2018 Dec 9 21:34:00	2018 Dec 10 06:59:38
63.77	3693.17285 $^{+0.00021}_{-0.00021}$	2019 Feb 11 06:43:16	2019 Feb 11 16:08:53	2019 Feb 12 01:34:31
63.77	3756.94707 $^{+0.00023}_{-0.00022}$	2019 Apr 16 01:18:09	2019 Apr 16 10:43:46	2019 Apr 16 20:09:24
60.23	3558.53829 $^{+0.00022}_{-63.40115}$	2018 Sep 29 15:29:24	2018 Sep 30 00:55:08	2018 Sep 30 10:20:38
60.23	3618.7695 $^{+0.00024}_{-66.5712}$	2018 Nov 28 21:02:20	2018 Nov 29 06:28:04	2018 Nov 29 15:53:34
60.23	3679.00071 $^{+0.00025}_{-69.74124}$	2019 Jan 28 02:35:17	2019 Jan 28 12:01:00	2019 Jan 28 21:26:31
60.23	3739.23191 $^{+0.00027}_{-72.91127}$	2019 Mar 29 08:08:13	2019 Mar 29 17:33:57	2019 Mar 30 02:59:27
60.23	3799.46311 $^{+0.00029}_{-76.08131}$	2019 May 28 13:41:09	2019 May 28 23:06:53	2019 May 29 08:32:23
57.06	3609.25939 $^{+0.00019}_{-0.00019}$	2018 Nov 19 08:47:54	2018 Nov 19 18:13:31	2018 Nov 20 03:39:08
57.06	3666.32054 $^{+0.0002}_{-0.0002}$	2019 Jan 15 10:15:57	2019 Jan 15 19:41:34	2019 Jan 16 05:07:11
57.06	3723.38169 $^{+0.00022}_{-0.00021}$	2019 Mar 13 11:44:01	2019 Mar 13 21:09:38	2019 Mar 14 06:35:14
57.06	3780.44284 $^{+0.00023}_{-0.00023}$	2019 May 9 13:12:04	2019 May 9 22:37:41	2019 May 10 08:03:17

HIP 41378 will also be in the field of view of *TESS* camera 1 in sector 7 (calculated using the Web Tess Viewing tool²¹) from 2019 July 1 to 2019 April 2. This time frame lines up with transits of six of the possible periods of planet d (53, 55, 58, 74, 111, and 222 days) and four of the possible periods of planet f (57, 60, 77, 120 days). This viewing window also coincides with an expected transit of planet c, allowing us to add an additional point to the TTV analysis separated by ~ 200 days from the previous measurement.














The authors would like to direct the reader to Becker et al. (2019), which also presents an updated analysis of the HIP 41378 system.

This work is based in part on observations made with the *Spitzer Space Telescope*, which is operated by the Jet Propulsion Laboratory, California Institute of Technology under a contract with NASA. Support for this work was provided by NASA through an award issued by JPL/Caltech. D.B. and I.J.M.C. acknowledge support from NSF AAG grant 1616648, D.B. acknowledges support from an NSERC PGS-D scholarship, and I.J.M.C. acknowledges support from NASA K2 GO grants NNH15ZDA001N-15-K2GO4_2-0018 and NNH16ZDA001N-16-K2GO5_2-0005.

The authors wish to recognize and acknowledge the very significant cultural role and reverence that the summit of Maunakea has always had within the indigenous Hawaiian community. We are most fortunate to have the opportunity to conduct observations from this mountain.

Facility: *Kepler*, *K2*, *Spitzer*, Keck I, *Gaia*.

ORCID iDs

David Berardo  <https://orcid.org/0000-0001-6298-412X>
 Ian J. M. Crossfield  <https://orcid.org/0000-0002-1835-1891>
 Erik Petigura  <https://orcid.org/0000-0003-0967-2893>
 Jessie Christiansen  <https://orcid.org/0000-0002-8035-4778>
 David R. Ciardi  <https://orcid.org/0000-0002-5741-3047>
 Courtney Dressing  <https://orcid.org/0000-0001-8189-0233>
 Benjamin J. Fulton  <https://orcid.org/0000-0003-3504-5316>
 Thomas P. Greene  <https://orcid.org/0000-0002-8963-8056>
 Kevin Hardegree-Ullman  <https://orcid.org/0000-0003-3702-0382>
 Stephen R. Kane  <https://orcid.org/0000-0002-7084-0529>
 John Livingston  <https://orcid.org/0000-0002-4881-3620>
 Farisa Morales  <https://orcid.org/0000-0001-9414-3851>
 Joshua E. Schlieder  <https://orcid.org/0000-0001-5347-7062>

References

- Becker, J. C., Vanderburg, A., Adams, F. C., Rappaport, S. A., & Schwengeler, H. M. 2015, *ApJL*, **812**, L18
 Becker, J. C., Vanderburg, A., Rodriguez, J. E., et al. 2019, *AJ*, **157**, 19
 Beichman, C. A., Giles, H. A. C., Akeson, R., et al. 2018, *AJ*, **155**, 158
 Beuzit, J.-L., Feldt, M., Dohlen, K., et al. 2006, *Msngr*, **125**, 29
 Bradley, L., Sipocz, B., Robitaille, T., et al. 2018, *astropy/photutils*: v0.5, Zenodo, doi:10.5281/zenodo.1340699
 Chen, J., & Kipping, D. 2017, *ApJ*, **834**, 17
 Choi, J., Dotter, A., Conroy, C., et al. 2016, *ApJ*, **823**, 102
 Crossfield, I. J. M. 2016, arXiv:1604.06458
 Dawson, R. I., & Johnson, J. A. 2012, *ApJ*, **756**, 122
 Dawson, R. I., Lee, E. J., & Chiang, E. 2016, *ApJ*, **822**, 54

²¹ <https://heasarc.gsfc.nasa.gov/cgi-bin/tess/webtess/wtv.py>

- Deming, D., Knutson, H., Kammer, J., et al. 2015, *ApJ*, 805, 132
- Fischer, D. A., Marcy, G. W., Butler, R. P., et al. 2008, *ApJ*, 675, 790
- Foreman-Mackey, D., Hogg, D. W., Lang, D., & Goodman, J. 2013, *PASP*, 925, 306
- Fulton, B. J., & Petigura, E. A. 2018, *AJ*, 156, 264
- Gaia Collaboration, Brown, A. G. A., Vallenari, A., et al. 2018, *A&A*, 616, A1
- Gaia Collaboration, Prusti, T., de Bruijne, J. H. J., et al. 2016, *A&A*, 595, A1
- Kane, S. R., Hill, M. L., Kasting, J. F., et al. 2016, *ApJ*, 830, 1
- Kipping, D. M. 2013, *MNRAS*, 435, 2152
- Kreidberg, L. 2015, *PASP*, 127, 1161
- Livingston, J. H., Crossfield, I. J. M., Werner, M. W., et al. 2019, *AJ*, 157, 102
- Macintosh, B., Troy, M., Doyon, R., et al. 2006, *Proc. SPIE*, 6272, 62720N
- Morton, T. D. 2015, isochrones: Stellar model grid package, Astrophysics Source Code Library, ascl:1503.010
- Pecaut, M. J., & Mamajek, E. E. 2013, *ApJS*, 208, 9
- Schlieder, J. E., Crossfield, I. J. M., Petigura, E. A., et al. 2016, *ApJ*, 818, 87
- Seager, S., & Mallén-Ornelas, G. 2003, *ApJ*, 585, 1038
- Shporer, A., Winn, J. N., Dreizler, S., et al. 2010, *ApJ*, 722, 880
- Sullivan, P. W., Winn, J. N., Berta-Thompson, Z. K., et al. 2015, *ApJ*, 809, 77
- Vanderburg, A., & Johnson, J. A. 2014, *PASP*, 126, 948
- Vanderburg, A., Becker, J. C., Kristiansen, M. H., et al. 2016, *ApJL*, 827, L10
- Villanueva, S., Jr., Gaudi, B. S., Pogge, R. W., et al. 2018, *PASP*, 130, 015001
- Weiss, L. M., Marcy, G. W., Petigura, E. A., et al. 2018, *AJ*, 155, 48